Virtual deployment of pipeline flow diverters in cerebral vessels with aneurysms to understand thrombosis.

Leonardo Flórez-Valencia[1], Eduardo E. Dávila Serrano[2], Juan G. Riveros Reyes[1], Olivier Bernard[2], Jonas Latt[3], Orestis Malaspinas[3,4], Bastien Chopard[3], Guy Courbebaisse[2], and Maciej Orkisz[2]

[1] Grupo Takina, Departamento de Ingeniería de Sistemas, Pontificia Universidad Javeriana, Bogotá, Colombia
florez-l@javeriana.edu.co
[2] Université de Lyon, CREATIS; CNRS UMR 5220; INSERM U 1044; INSA-Lyon; Université Lyon 1, France
[3] University of Geneva, Computer Science Department, 1211 Geneva 4, Switzerland
[4] Institut Jean le Rond d'Alembert, CNRS UMR 7190; Université Pierre et Marie Curie - Paris 6, 4 place Jussieu - case 162, F-75252, France

Abstract. We present a prototype software to virtually deploy pipeline flow diverting stents in intracranial vessels with aneurysms. The final objective is to understand the biological and biomechanical mechanisms underlying the stent-induced clot formation within the aneurysm. The weaving pattern of the selected pipeline stent is described w.r.t. cylindrical coordinates. Patient-specific 3D vascular geometry is extracted by a level-set image segmentation algorithm. A deformable cylindrical simplex mesh model is used to simulate the virtual stent positioning. A continuous Right Generalized Cylinder model is then used to obtain the mapping of the stent geometry onto the deformed cylindrical surface. Meshes representing the vessel/aneurysm surface and the filaments of the stent are used as input to simulate the fluid dynamics without and with the virtual stent. Lattice Boltzmann method is used to solve the equations. We show preliminary visual results on a first patient.

1 Introduction

Rupture risk of intracranial aneurysms (IA) has been studied at length [23,25,7]. However, very little is known about the healing mechanism, namely the formation of a clot (thrombus) inside the aneurysm cavity after insertion of a stent. Spontaneous thrombosis has been observed and modeled in giant aneurysms [6], where it can reduce the risk of rupture and lead to healing, but has never been reported in smaller IA that can nevertheless disrupt with catastrophic consequences. In medical practice, various blood-flow diverting stents are used in an attempt to induce the thrombus onset. The physicians empirically choose the stent parameters and often superimpose more than one stent in order to achieve what they expect to be the appropriate density of the filaments.

Our project [4] aims at modeling multiscale interactions between biological and hemodynamic processes to better understand the thrombosis mechanisms in IA and how blood-flow diverting stents can influence the healing process. Here we focus on the part of the project related to the virtual insertion of a pipeline stent into the patient's vessels. Similarly to previous initiatives [10,12,17], our workflow starts by a patient's image segmentation to extract the vessel geometrical shape represented by a discrete three-dimensional mesh bound and a central axis. While the mesh represents the vessel wall, the axis is used to guide an interactive insertion of a virtual catheter that delivers the stent. Once the catheter has reached the delivery zone, a deformation algorithm "inflates" the model of the stent until it "touches" the vessel wall. A combination of the meshes representing the vessel endoluminal surface and the stent is then used as input for CFD simulations. The deformation of the stent model is controlled by internal and external forces. The former preserve the continuity and smoothness of the stent shape. They often are quite generic, based on parametric surface derivatives, like in [10], where a classical active surface model has been used. More sophisticated models, can include internal forces based on real properties of the filaments [17]. The external forces can include a "balloon" force that "inflates" the model, a force that attracts the model towards the edges in the image and/or a collision force that stops the evolution on the boundary of a presegmented vessel. We use the same deformable cylindrical simplex model as in [17], but we focus on a different type of stents, namely the pipeline flow diverters. Our prototype is based on CreaTools software development framework [1,2].

2 Method

The virtual insertion of the stent into the patient's vessels can be subdivided into three steps: preprocessing, generation of stent geometrical characteristics and virtual stent deployment. These steps build on two generic models that will be described prior to the presentation of the actual simulation.

2.1 Models

Static representations use a continuous model denoted by RGC (right generalized cylinder), whereas dynamic representations use a deformable model denoted by cylindrical simplex mesh.

Right Generalized Cylinder model. The RGC model [5,11,21] puts together a *continuous* axis and a *continuous* surface calculated from a stacking of discrete planar contours orthogonal to the centerline. It assumes that the cylinder segments between two contours are short enough to be described by constants. The very first contour of the stacking is described by its Fourier coefficients, the number of coefficients depending on the details desired. When only two coefficients are used, the cross-sectional shape of the cylinder is forced to be elliptical or

circular. The very first point of the axis is defined by an associated orthonormal frame, possibly rotated w.r.t. the Frenet frame. The axial shape (*i.e.* the evolution of the reference frame) between the consecutive contours is defined by a constant curvature, torsion and rotation, which means that such an axis segment is a helix. As for the Fourier coefficients describing the contours, they are assumed to evolve linearly within a given cylinder segment, so only their finite difference between two contours is needed to describe the surface of the whole segment, regardless its complexity. The RGC model has been used in the past both to generate computer phantoms of various cylindrical shapes and to reconstruct such shapes from image data, when associated with appropriate contour extraction method and tracking strategy.

Deformable Cylindrical Simplex mesh. This *discrete* model also associates an axis and a surface. Both are represented using N-dimensional k-simplex meshes [9,12,13], where each vertex has exactly $k+1$ neighbor vertices. To represent the surface we use a 3D 2-simplex mesh $\mathcal{S}_v = \left\{\mathbf{g}_j \in \mathbf{R}^3, 0 \leq j < J\right\}$, while a 3D 1-simplex mesh with radius r_i associated to each vertex $\mathbf{a}_i$ is used to represent the axis $\mathcal{C}_v = \left\{(\mathbf{a}_i, r_i) \in \mathbf{R}^3 \times \mathbf{R}^+, 0 \leq i < I\right\}$. The complete model includes $\mathcal{C}_v$, $\mathcal{S}_v$ and the spatial relationships between $\mathbf{a}_i$ and $\mathbf{g}_j$. According to the classical deformable model framework, the mesh deformation is controlled by two types of forces: 1) internal $\mathbf{f}_{int}(\mathbf{g}_j)$, the computation of which benefits from the specificity of the simplex-meshes formalism and uses a criterion enforcing the regularity of the surface curvature, and 2) external $\mathbf{f}_{ext}(\mathbf{g}_j)$ that can attract the model towards the edges in the image or push it outwards like a balloon force. Each surface vertex $\mathbf{g}_j$ is associated with the 3 closest axis vertices $\mathbf{a}_k$. When the surface undergoes a deformation, the axis bends accordingly through an external force $\mathbf{f}_{ext}(\mathbf{a}_k)$ resulting from the surface forces reported onto the axis. Conversely, the axis bending is reported onto the surface to ensure a homogeneous deformation behavior of the cylinder surface. The corresponding external force acting on the surface is a weighted sum of an axial component $\mathbf{f}_{axial}(\mathbf{g}_j)$ (each vertex tends to follow the axis global motion) and of a radial component $\mathbf{f}_{radial}(\mathbf{g}_j)$ (each vertex tends to align on a circle around the axis). The advantages of simplex-meshes are: fast computation (particularly when associated with QuadEdge implementation [15], possibility of managing the surface and the centerline within the same formalism, easy control of the 3D continuity and regularity of the surface, duality with triangulation (easy display). This model is therefore very well suited to the simulations.

2.2 Preprocessing

The preprocessing begins by manually selecting a volume of interest (VOI) within the original image, both to facilitate the visualization and interaction at the subsequent stages of the workflow, and to reduce the computational time. Subsequently, a segmentation algorithm automatically separates the aneurysm and vessels from the remaining tissues within the VOI. Various vessel segmentation

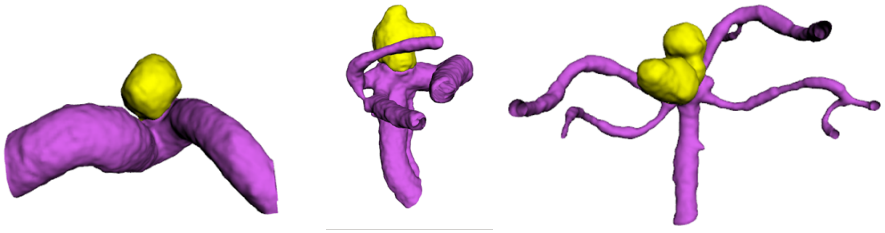

Fig. 1. Segmentation results with the aneurysm separated from the vessels.

algorithms can be tested at this stage. We have implemented three different level-set techniques based on different data attachment terms: optimal threshold [14], minimal variance [8] and a term specifically devised to extract thin structures [16]. Each of these methods only needs an interactive definition (click) of an initial point inside the aneurysm to start the segmentation process. The separation between the aneurysm and the vessels is performed by an improved version of the subjective-surface method from Sarti et al. [24] (Fig. 1).

Our simulation of the stent insertion needs the centerline of the vessel of interest to be used as guide-wire. Since some vessel-segmentation methods directly provide the centerline (see [18] for an overview), while others do not, we have included an option to extract the necessary centerline from the binary result of the segmentation. Actually, the extraction is performed within the segmented vessels after the exclusion of the aneurysm by the subjective-surface method. Usually, more than one vessel is present in the VOI. The vessel of interest is interactively selected by pointing its ends. The centerline is extracted between these points. To be consistent with the remaining steps, we used the formalism of the RGC model, although many other solutions might fit this step. Hence, contours of the binary vessel are progressively extracted, starting from one of the ends, and the RGC parameters are deduced from the consecutive contour pairs. In this way, both a centerline and a continuous surface representation closely fitting the vessel boundary become available.

2.3 Generating the stent geometry

Let us note that the stent geometry is needed at the very end of the virtual deployment process. Until that stage, only the overall cylindrical shape of the stent is manipulated, in order to simplify the interaction and display. However, both to graphically represent the final detailed shape of the stent, and to generate the corresponding mesh needed for further simulations, the actual geometry of the stent is to be defined. At that stage, the radius R and length L of the deployed stent (possibly different from the nominal values R_N and L_N) are already known. Before displaying a stent inserted into vascular structures and bent according to the vessel axial shape, it is necessary to generate a representation of a right stent, i.e. with an axis represented by a straight line.

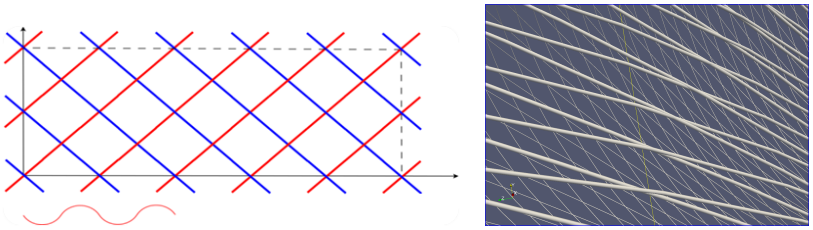

Fig. 2. Generating the stent geometry: schematic planar representation of filament centerlines (left), close-up of the 3D representation (right).

Here, the focus is on a specific type of pipeline stents, where the filaments are interlaced according to a predefined pattern. In addition to the interlacing pattern, a given stent is characterized by the number of filaments and by their thickness $2r$. We reproduce these characteristics in three steps. All these steps are performed using a planar rectangle $2\pi R \times L$ that bijectively maps onto a cylinder of length L and radius R. First, the centerlines of the filaments are drawn on the rectangle (Fig. 2 left). Each loop of each filament is represented by a straight line segment and these lines are parallel for all filaments turning in the same sense. These lines cross those representing the filaments that turn in the opposite sense. The angles formed by these lines between them and with the borders of the rectangle can easily be deduced from the number of filaments and the rectangle dimensions [20]. Second, the position of the lines is modulated in the direction orthogonal to the rectangle surface, to take into account the interlacing pattern. In the simplest case, where each filament alternatively passes above then below the other crossed filaments, this modulation can be sinusoidal with a magnitude equal to the filament radius r. The last step is to generate a cylindrical mesh around each filament's centerline, (Fig. 2 right).

2.4 Virtual stent deployment

Simulating the stent deployment involves two main steps: interactive choice of the delivery location and automatic "inflation" of the stent until its size fits the vessel diameter. An additional step maps the representation of the interlaced filaments onto the cylinder representing the deployed stent. While the first step is very simple and consists in sliding a thin cylinder along the vessel centerline until the desired location, as described in [12], the second step differs from the seminal work [12,13], although it also uses the same deformable cylindrical simplex model. As the stent is expected to keep the axial shape of the vessel, we relaxed the external force $\mathbf{f}_{ext}(\mathbf{a}_k)$. In the generic implementation of the model, this force transmits onto the axis a combination of external forces acting on the surface. Additionally, in the seminal work, the external force attracting the surface of the model was linked to the image intensity gradient. In our case, the vessels are already segmented, so this force was replaced by a "balloon" force that "inflates" the surface mesh. The inflation does not involve axial displacements of

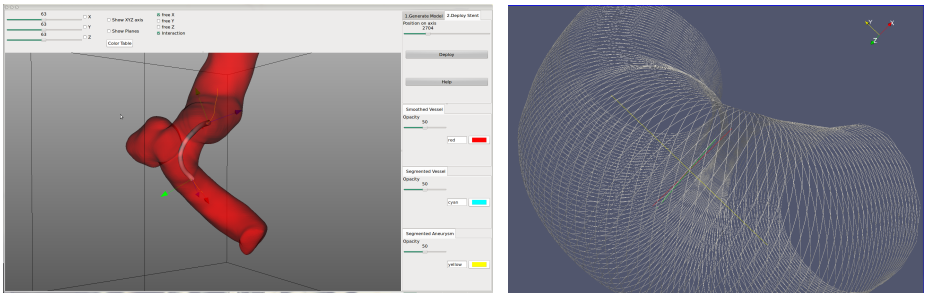

Fig. 3. Stent deployment. Left: graphical user interface with a display of a segmented vessel, aneurysm and folded stent placed along the centerline. Right: unfolded stent.

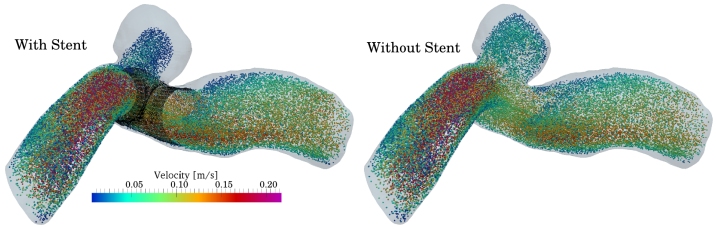

Fig. 4. Example of CFD simulation with and without stent.

the surface nodes, so the force component $\mathbf{f}_{axial}(\mathbf{g}_j)$ also became useless, while the component $\mathbf{f}_{radial}(\mathbf{g}_j)$ is driven by the nominal radius R_N and enforces a circular cross-sectional shape. The evolution of the deformable model stops when one of the surface nodes collides with the vessel boundary. The final radius, length and axial shape of the simplex mesh are used to calculate a continuous cylindrical surface described by the RGC model. This in turn is used to infer the actual spatial coordinates of the filaments, according to the bijective mapping between the previously described planar representation and the cylindrical surface (Fig. 3). The resulting mesh representation is combined with the mesh representing the vascular surface, so that the whole can be used to simulate the blood flow modified by the presence of the stent.

3 Results

The first experiments aimed at demonstrating the correct interoperability of all the components of the workflow leading to plausible results. To this purpose, we first simulated the insertion of a pipeline stent with 48 wires, filament diameter 0.027 mm, $R_N = 1.36$ mm then the Navier-Stokes equations were solved by using the lattice Boltzmann method [22] implemented in Palabos software [3]. More precisely, 3D and 4D BGK lattice Boltzmann codes were used with the Carreau-Yasuda constitutive law [19]. Figure 4 shows a result of a BGK D3Q19 simulation with the following parameters: mean velocity 0.05 m/s, Reynolds number 200,

inlet diameter 4 mm, number of lattice grid nodes larger than 40 million, number of cores for parallel computation 120. Particles virtually injected into the blood are displayed with colors representing their velocity. As expected, the presence of a virtual stent significantly reduced the velocities within the aneurysmal cavity. Indeed, densely woven filaments constitute an obstacle for the blood flow, despite their very tiny diameters. The calculated surface coverage was 31.1%.

Our numerical simulation fully resolved the structure of the stent and the flow around the filaments of the stent, unlike a more common approach, in which the effect of the stent was approximated by a model of porous media. A huge resolution of the flow mesh was necessary to achieve this aim, because the diameter of the stent filaments differs from the diameter of the artery by three orders of magnitude. The code used for the simulations was efficiently parallelized: not only the actual CFD simulation, but also the generation of the computational mesh and the post-processing of the data.

4 Conclusions and Perspectives

We have implemented a complete workflow to perform a virtual stenting of intracranial aneurysms using pipeline flow diverters. The prototype used generic components both to construct the models and to build up the graphical user interface. The first results demonstrated a good interoperability of these components and the resulting meshes proved to be exploitable in CFD simulations. These simulations have been carried out using software based on the Lattice Boltzmann method. The resulting flow patterns clearly depict the influence of the stent on the blood velocities within the aneurysm. These results now need to be correlated with the findings in the biological and clinical domains. It is expected that these experiments will allow us to use the simulations to predict *a priori* the outcome of various stenting strategies.

Acknowledgements

This work has been partly funded by the E.C. via VPH STREP Thrombus FP7-ICT-2009-6-269966, as well as by the ECOS Nord Commitee grant C11S01.

References

1. `http://toolkit.vph-noe.eu/home/tools/imaging/creatools.html`.
2. `http://www.creatis.insa-lyon.fr/site/en/CreaTools_home`.
3. `http://www.palabos.org`.
4. `http://www.thrombus-vph.eu`.
5. J. Azencot and M. Orkisz. Deterministic and stochastic state model of right generalized cylinder (RGC-sm): application in computer phantoms synthesis. *Graph. Models*, 65(6):323–350, 2003.
6. R. D. Brownlee, B. I. Tranmer, R. J. Sevick, G. Karmy, and B. J. Curry. Spontaneous thrombosis of an unruptured anterior communicating artery aneurysm : an unusual cause of ischemic stroke. *Stroke*, 26(10):1945–1949, 1995.

7. J. R. Cebral, M. A. Castro, J. E. Burgess, R. S. Pergolizzi, M. J. Sheridan, and C. M. Putman. Characterization of cerebral aneurysms for assessing risk of rupture by using patient-specific computational hemodynamics models. *Am. J. Neuroradiol.*, 26(10):2550–2559, 2005.
8. T. F. Chan and L. A. Vese. Active contours without edges. *IEEE Trans. I.P.*, 10(2):266–277, 2001.
9. H. Delingette. General object reconstruction based on simplex meshes. *Int. J. Comput. Vision*, 32(2):111–146, 1999.
10. J. Egger, S. Grosskopf, C. Nimsky, T. Kapur, and B. Freisleben. Modeling and visualization techniques for virtual stenting of aneurysms and stenoses. *Comput. Med. Imaging Graph.*, 36(3):183–203, 2012.
11. L. Flórez-Valencia, J. Azencot, and M. Orkisz. Algorithm for blood-vessel segmentation in 3D images based on a right generalized cylinder model: application to carotid arteries. In *Int. Conf. Comput. Vision Graph.: Part I, Warsaw, Poland*, volume 6374 of *LNCS*, pages 27–34, Berlin, Heidelberg, 2010. Springer-Verlag.
12. L. Flórez-Valencia, J. Montagnat, and M. Orkisz. 3D graphical models for vascular-stent pose simulation. *Mach. Graph. Vis.*, 13(3):235–248, January 2004.
13. L. Flórez-Valencia, J. Montagnat, and M. Orkisz. 3D models for vascular lumen segmentation in MRA images and for artery-stenting simulation. *Innov. Technol. Biol. Med. - IRBM*, 28(2):65–71, 2007.
14. R. Gan, W. C. K Wong, and A. C. S. Chung. Statistical cerebrovascular segmentation in three-dimensional rotational angiography based on maximum intensity projections. *Med. Phys.*, 32(9):3017–3028, 2005.
15. A. Gouaillard, L. Flórez-Valencia, and E. Boix. ItkQuadEdgeMesh: a discrete orientable 2-manifold data structure for Image Processing. *Insight Journal*, 2006.
16. M. Holtzman-Gazit, R. Kimmel, N. Peled, and D. Goldsher. Segmentation of thin structures in volumetric medical images. *IEEE Trans. I.P.*, 15(2):354–363, 2006.
17. I. Larrabide, M. Kim, L. Augsburger, M. C. Villa-Uriol, D. Rüfenacht, and A. Frangi. Fast virtual deployment of self-expandable stents: method and in vitro evaluation for intracranial aneurysmal stenting. *MedIA*, 16(3):721–730, 2012.
18. D. Lesage, E. D. Angelini, I. Bloch, and G. Funka-Lea. A review of 3D vessel lumen segmentation techniques: models, features and extraction schemes. *MedIA*, 13(6):819–845, 2009.
19. O. Malaspinas, G. Courbebaisse, and M. O. Deville. Simulation of a generalized Newtonian fluid by the Lattice Boltzmann Method. *Int. J. Modern Phys. C*, 18(12):1939–1949, 2007.
20. P Mortier, M De Beule, D Van Loo, P Verdonck, and B Verhegghe. Parametric stent design using pyFormex. In *ASME 2008 Summer Bioeng. Conf.*
21. M. Orkisz, L. Flórez-Valencia, and M. Hernández Hoyos. Models, algorithms and applications in vascular image segmentation. *Mach. Graph. Vis.*, 17(1):5–33, 2008.
22. R. Ouared and B. Chopard. Lattice Boltzmann simulations of blood flow: non-Newtonian rheology and clotting processes. *J. Stat. Phys.*, 121(1-2):209–221, 2005.
23. G. J. E. Rinkel, M. Djibuti, A. Algra, and J. van Gijn. Prevalence and risk of rupture of intracranial aneurysms: a systematic review. *Stroke*, 29(1):251–256, 1998.
24. A. Sarti, R. Malladi, and J. A. Sethian. Subjective surfaces: a geometric model for boundary completion. *Int. J. Comput. Vision*, 46(3):201–221, 2002.
25. D. O. Wiebers. Unruptured intracranial aneurysms: natural history, clinical outcome, and risks of surgical and endovascular treatment. *The Lancet*, 362(9378):103–110, 2003.